Algorithm Theoretical Basis Document for Land Surface Temperature (LST)

PRODUCTS: LSA-002 (ELST)

The EUMETSAT Network of Satellite Application Facilities

LSA SAF Land Surface Analysis

Reference Number:	SAF/LAND/IM/ATBD_ELST/1.0
Issue/Revision Index:	Issue 1.0
Last Change:	28/10/2016

DOCUMENT SIGNATURE TABLE

	Name	Date	Signature
Prepared by :	I. Trigo, S. Freitas, J. Bioucas-Dias, C. Barroso, I. Monteiro, P. Viterbo, J.P. Martins		
Approved by :	Land SAF Project Manager (IPMA)		

DOCUMENTATION CHANGE RECORD

Issue / Revision	Date	Description:
Version 1.0	19/06/2009	Update of LST uncertainty estimations
Version 1.1	8/04/2016	Include reference to LSA-050: re-processed SEVIRI LST product. Refer LSA-002
Version 1.2	28/10/2016	Modifications suggested in ORR_EPS: - Algorithm for AVHRR/Metop LST and SEVIRI/MSG LST described in separated documents. - Added note on large scale systematic uncertainties possibly affecting LST products (last paragraph of section 4.5). - Reference to snow/ice emissivity included in section 4.3. - Improved description of ELST re-gridding procedure (end of section 5). - Clarified that only the primary satellite is used (1st paragraph in section 1).

DISTRIBUTION LIST

Internal Consortium Distribution		
Organisation	**Name**	**No. Copies**
IPMA	Isabel Trigo	
IPMA	Isabel Monteiro	
IDL	Carlos da Camara	
IPMA	Sandra Coelho	
IPMA	Carla Barroso	
IPMA	Pedro Diegues	
IPMA	Teresa Calado	
IPMA	Pedro Ferreira	
IPMA	Ricardo Torres	
IMK	Folke-S. Olesen	
IMK	Frank Goettsche	
IMK	Ewa Kabsch	
MF	Jean-Louis Roujean	
MF	Dominique Carrer	
MF	Dominique Carrer	
RMI	Françoise Meulenberghs	
RMI	Arboleda Alirio	
RMI	Nicolas Ghilain	
FMI	Niilo Siljamo	
UV	Joaquin Melia	
UV	F. Javier García Haro	
UV/EOLAB	Fernando Camacho	
UV	Aleixander Verger	

External Distribution		
Organisation	**Name**	**No. Copies**
EUMETSAT	Frédéric Gasiglia	
EUMETSAT	Cleber Balan	
EUMETSAT	Lorenzo Sarlo	
EUMETSAT	Lothar Schueller	
EDISOFT	Tiago Sepúlveda	
EDISOFT	Joana Rosa	
EDISOFT	Joaquim Araujo	
GMV	Mauro Lima	

Steering Group Distribution		
Nominated by:	**Name**	**No. Copies**
IPMA	Pedro Viterbo	
EUMETSAT	Lorenzo Sarlo	
EUMETSAT	Lothar Schueller	
EUMETSAT	Christopher Hanson	
EUMETSAT	Harald Rothfuss	
STG/AFG (USAM)	Francesco Zauli	
MF	Jean-François Mahfouf	
RMI	Rafiq Hamdi	
KIT	Johannes Orphal	
VITO	Bart Deronde	

Table of Contents

DOCUMENT SIGNATURE TABLE 2
DOCUMENTATION CHANGE RECORD 2
1. Introduction 7
2. Data Description 8
2.1. AVHRR on-board Metop 8
2.2. Calibration/Verification Database 8
2.3. Radiative Transfer Simulations 10
3. The Land-SAF ELST Algorithm 11
3.1. Generalized Split-Windows 11
3.2. Calibration/Validation of the GSW Algorithm 12
4. Error Propagation 13
4.1. Framework 13
4.2. Impact of Sensor Noise 15
4.3. Impact of uncertainties in Surface Emissivity 15
4.4. Uncertainties in forecasts of atmospheric water vapour content 16
4.5. Uncertainty of LST Retrievals 17
5. Daily Composites of AVHRR/Metop LST – LSA-002 18
6. Concluding Remarks 19
7. References 21

List of Tables

Table 1 Central wavenumber and band-correction coefficients for AVHRR thermal windows channels onboard Metop-A and Metop-B, respectively (EUMETSAT, 2011). 11
Table 2 Uncertainty values considered for surface emissivity of Metop channels 4 and 5. 16
Table 3 Fraction of Vegetation Cover attributed per land cover class. 18
Table 4- Description of LST/AVHRR Quality Flag information..... 19

List of Figures

Figure 1 Spectral response functions of AVHRR thermal windows channels (5 and 4), centred at 10.8 and 11.9 μm, respectively, on-board Metop1 and Metop2. 8
Figure 2 Main properties of the calibration database for AVHRR/Metop LST: a) TCWV distribution, b) T_Skin distribution, c) Bivariate TCWV/T_Skin distribution and d) geographical distribution. 9
Figure 3 Assessment of the ELST Generalized Split-Windows algorithm against the validation databased: root mean square differences (ºC) per classes of Total Column Water vapour (x-axis) and view zenith angle (y-axis), considering the coefficients calibrated for Metop-A and Metop-B response functions, respectively. 12
Figure 4 Uncertainty in LST estimates, measured as the RMSD (ºC) between retrieved LST and the validation database true value, considering: (a) the input data are error-free; (b) the sensor noise; (c) the uncertainty associated to total column water vapour forecasts; (d) uncertainty in surface emissivity, for cases where it lies between 0.8 and 0.95 (mostly barren surfaces); (e) uncertainty in surface emissivity, for cases where it lies between 0.95 and 0.98 (sparsely to moderately vegetated surfaces); (f) uncertainty in surface emissivity, for cases where it is higher than 0.95 (vegetated and/or moist surfaces or inland water bodies). The lower row represents total uncertainty, for the emissivity types described above. The results are presented for combinations of W (x-axis) and view zenith angle (y-axis), for Metop-B algoritm. 14
Figure 8 Example of one Daytime LST estimate (ºC) and respective quality flag. 20
Figure 9 Example of one Night-time LST estimate (ºC) and respective quality flag..... 21

1. Introduction

This document details the algorithm used for the retrieval of Land Surface Temperature (LST) from the Advanced Very High Resolution Radiometer (AVHRR) on-board EUMETSAT polar system satellites, the Metop series. The methodology detailed here applies to daily AVHRR LST product (LSA-002), following a very similar algorithm to that used for LSA SAF LST product derived from Meteosat Second Generation (with product identifiers LSA-001 and LSA-050). The LSA SAF ELST product is generated from observations gathered by the primary Metop satellite.

LST estimations from remotely sensed data are generally obtained from one or more channels within the thermal infrared atmospheric window from 8-to-13 μm (Dashet al., 2002). Operational LST retrievals often make use of split-window algorithms (e.g., Prata, 1993; Wan and Dozier, 1996), where LST is obtained through a semi-empirical regression of top-of-atmosphere (TOA) brightness temperatures of two pseudo-contiguous channels, i.e., the split-window channels. The Land-SAF LST algorithm is based on the generalised split-window (GSW) formulation initially developed for AVHRR and MODIS (Wan and Dozier, 1996), recalibrated taking into account AVHRR-3 channels. The error of LST retrievals via GSW depends on (i) the uncertainty of surface emissivity, (ii) the water vapour content of the atmosphere, and (iii) or the satellite view angle. Because the latter determines the total optical path, LST estimations are often limited to satellite zenith angles (SZA) below ~60º, where retrieval errors are still acceptable (e.g., Wan and Dozier, 1996; Sun and Pinker, 2003; Jiménez-Muñoz and Sobrino, 2006; Freitas et al., 2011; Martins et al, 2016). The LSA SAF AVHRR/Metop product is generated globally, for satellite zenith angles up to 60º.

2. Data Description

2.1. AVHRR on-board Metop

Metop satellites constitute the current EUEMTSAT polar system and amongst others, are equipped with the Advanced Very High Resolution Radiometer (AVHRR), which has a swath of about 2400km, providing Earth observations with view zenith angles (SZA) up to about 60º, and a spatial resolution at nadir of 1.1 km. AVHRR provides information on 6 channels, with two in the thermal infrared. As in the case of SEVIRI, the latter are centred at about 10.8 μm and 11.9 μm (Figure 1), respectively, and are used to derive LST.

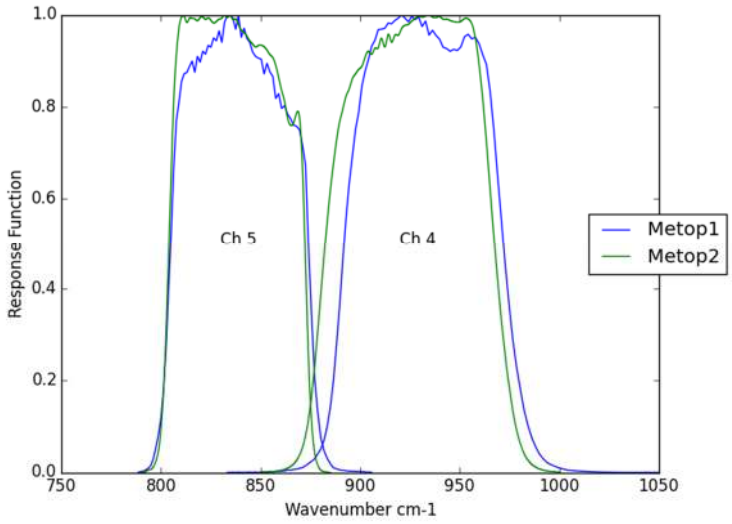


Figure 1 Spectral response functions of AVHRR thermal windows channels (5 and 4), centred at 10.8 and 11.9 μm, respectively, on-board Metop1 and Metop2.

2.2. Calibration/Verification Database

The calibration (and verification) of the GSW presented here relies on radiative transfer simulations of TOA brightness temperatures for AVHRR channels 4 and 5. The simulations are performed for the database of global profiles of temperature, moisture, and ozone compiled by Borbas et al. (2005) for clear sky conditions, and referred to as SeeBor. The database contains over 15,700 profiles taken from other datasets, such as NOAA88 (Seemann et al., 2003), TIGR-like (Chevallier, 2001), and TIGR (Chedin et al., 1996), that are representative of a wide range of atmospheric (clear sky) conditions over the whole globe. In addition, surface parameters such as skin temperatures (Tskin) and a landcover classification within the International Geosphere-Biosphere Programme ecosystem categories (IGBP) (Belward, 1996) are assigned to each profile. Skin temperature over land surfaces corresponds to LST in SeeBor and is estimated as a function of 2m temperature (T2m), and solar zenith and azimuth angles (Borbas et al. 2005).

The calibration database of the GSW for ELST takes into account that this is a global product. For this purpose, we consider a set of globally distributed atmospheric profiles with the properties described in Figure 3 (Martins et al., 2016). The calibration databased followed the following criteria:

1) First we define classes of T_{Skin}Tskin (from 200 K to 330 K in steps of 5 K) and TCWV from 0 to 6 cm in classes of 0.75 mm. A large enough number of profiles are selected from the SeeBor, ensuring that the all physically possible cases in the TCWV/Tskin phase state is fully covered (see Figure 3c).
2) For each of the selected profiles, we assign a new Tskin based on the ranges of Tskin - Tair to cover realistic ranges. The choice of the range of perturbations to apply is key to the performance of the LST algorithms. Here we considered a range of ±15K around Tair in steps of 5K.
3) Each of these conditions may be sensed from angles ranging from 0 (nadir view) to 60º in steps of 2.5º.
4) Emissivity range: values of ε10.8 (channel 4) from 0.93 to 1.0 in steps of 0.01; values of ε12.0 (channel 5) are based on departures from the former: -0.015 to 0.035 in steps of 0.01 (excluding cases where ε12.0 > 1$\epsilon_{12.0} > 1.0$).

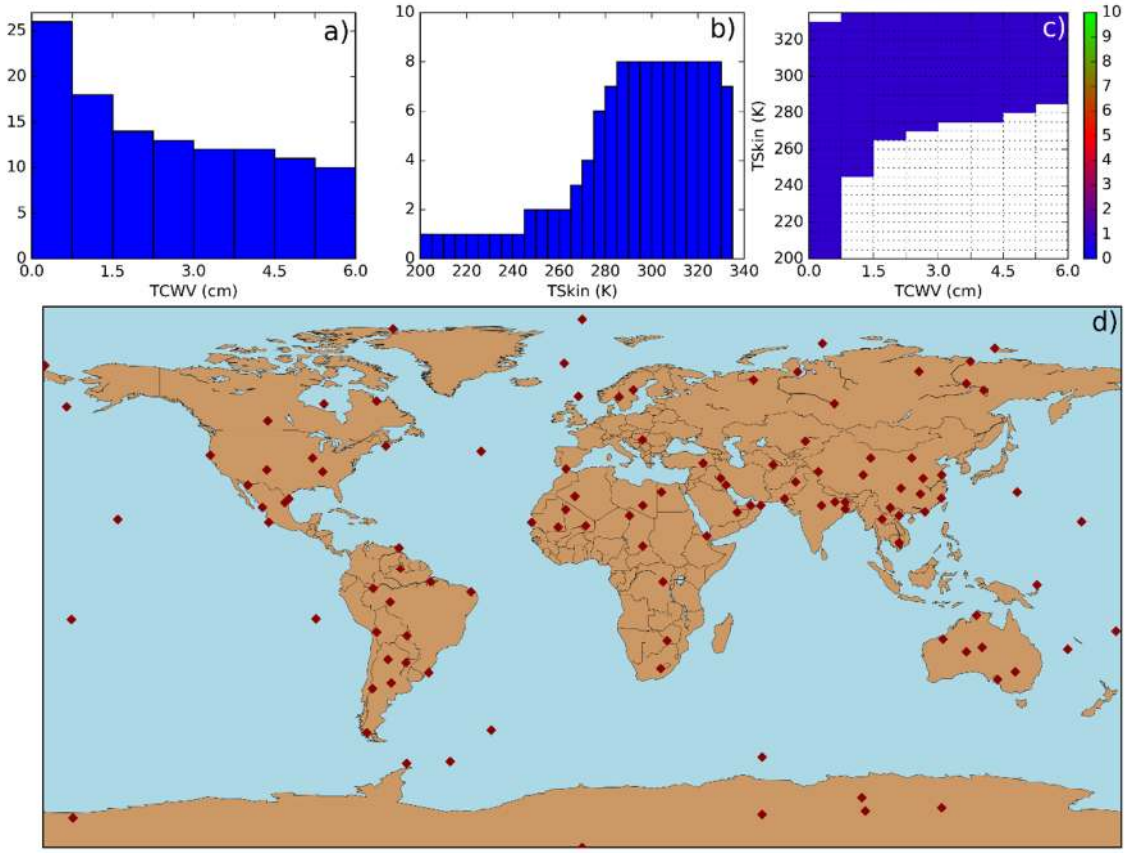


Figure 2 Main properties of the calibration database for AVHRR/Metop LST: a) TCWV distribution, b) T_Skin distribution, c) Bivariate TCWV/T_Skin distribution and d) geographical distribution.

The spatial distribution of SeeBor profiles selected to be part of the calibration database is shown in Figure 2d. The statistical distributions of skin temperature (or surface temperature), TCWV, as well as their join distributions are shown in Figure 2a, Figure 2b, and Figure 2c. The verification database will then be formed by all SeeBor profiles, excluding those selected for calibration purposes.

2.3. Radiative Transfer Simulations

The MODerate spectral resolution atmospheric TRANSsmittance algorithm (MODTRAN4) (Berk et al., 2000) provides a useful tool to quantify the radiation emitted by the surface within known atmospheric conditions that reaches a sensor operating in a specific spectral band. The radiance (L_ν) is estimated using MODTRAN4, for the bands corresponding to AVHRR channels 4 and 5, with a spectral resolution of 1 cm^{-1}. The integration of L_ν weighted by the i-th channel response function $\phi_{i,\nu}$, (see Figure 1) provides channel i effective radiance:

$$L_i = \frac{\int_{\nu_{i,1}}^{\nu_{i,2}} \phi_{i,\nu} L_\nu d\nu}{\int_{\nu_{i,1}}^{\nu_{i,2}} \phi_{i,\nu} d\nu} \quad (1)$$

where $\nu_{i,1}$ and $\nu_{i,2}$ are the lower and upper wavenumber boundaries of the channel, respectively; the integrals in (1) are estimated taking into account the full tabulated values of the response function $\phi_{i,\nu}$, i.e., between ν_1 = 830 cm^{-1} and ν_2 =1050 cm^{-1}, for channel 4, and between ν_1 = 760 cm^{-1} and ν_2 = 910.00 cm^{-1}, for channel 5.

The simulated AVHRR radiances for channel i, L_i, are then converted to equivalent black-body brightness temperatures (Tb_i) following the analytic formulation based on the Planck function (EUMETSAT, 2011):

$$Tb_i = A_i + B_i \frac{C_2 \nu_{ci}}{ln\left(1+\frac{C_1 \nu_{ci}^3}{L_i}\right)} \quad (2)$$

where $\nu_{i,c}$ is channel i central wavenumber (Table 1), C_1=2hc^2 and C_2=hc/k (h is the Plancks constant, c the speed of light and k the Boltzmann constant). The parameters A_i and B_i, shown in Table 1 for Metop-A and Metop-B, are band-correction coefficients, adjusted to AVHRR spectral response functions. The simulations of channel 4 and channel 5 brightness temperatures are then performed for both Metop-A and Metop-B, for the whole database (calibration and verification subsets) described in the previous sections.

Table 1 Central wavenumber and band-correction coefficients for AVHRR thermal windows channels onboard Metop-A and Metop-B, respectively (EUMETSAT, 2011).

Channel	Metop-A			Metop-B		
	ν_c (cm^{-1})	A (K)	B	ν_c (cm^{-1})	A (K)	B
Channel 4	926.566	-0.45749	1.0014	933.630	-0.50487	1.00136
Channel 5	836.344	-0.13685	1.0007	839.620	-0.38171	1.00114

3. The Land-SAF ELST Algorithm

3.1. Generalized Split-Windows

Several algorithms have been proposed to retrieve LST from remotely sensed thermal infrared data, e.g., Prata (1993), Dash et al. (2002), Sun and Pinker (2003), Sobrino and Romaguera (2004), Jiménez-Muñoz (2006), Coll et al., (2006), Yu et al. (2008) , Jiang amd Li (2008). The LSA SAF ELST is estimated following the same approach used for SEVIRI/MSG LST (Trigo et al., 2008b, Freitas et al., 2011, Martins et al., 2016) using a Generalized Split-Window (GSW) algorithm with a formulation similar to that first proposed by Wan and Dozier (1996) for MODIS. Thus, LST is as a function of TOA brightness temperatures of AVHRR channels 4 and 5 ($T_{10.8}$ and $T_{12.0}$, respectively):

$$LST = \left(A_1 + A_2\frac{1-\varepsilon}{\varepsilon} + A_3\frac{\Delta\varepsilon}{\varepsilon^2}\right)\frac{T_4+T_5}{2} + \left(B_1 + B_2\frac{1-\varepsilon}{\varepsilon} + B_3\frac{\Delta\varepsilon}{\varepsilon^2}\right)\frac{T_4-T_5}{2} + C + \Delta LST \quad (3)$$

where ε is the average of the two channels surface emissivities, Δε their difference ($\varepsilon_{10.8}$ - $\varepsilon_{12.0}$), while A_j, B_j, (j = 1,2,3) and C are the GSW coefficients obtained by fitting equation (3) to the calibration data described above, and ΔLST is the model error; for each class of water vapour W and SZA Ψ, a set of coefficients A_j, B_j, C is inferred by minimizing the the l_2-norm of the model error ΔLST. The GSW algorithm is applied to clear sky pixels only. In the Land-SAF, cloud removal is performed using the software developed by the Nowcasting (NWC) SAF, which is based on multispectral threshold technique applied to visible, near-infrared, and thermal atmospheric window AVHRR channels, for each pixel of the image (Dybbroe et al, 2005).

A relevant factor in the selection of the algorithm was its expected reliability for operational LST retrievals, both in terms of expected accuracy and timeliness. The latter favours the use of semi-empirical relationships between LST and TOA brightness temperatures, which are computationally efficient and free of the convergence problems of direct emissivity and temperature retrieval methods (e.g., Faysash and Smith, 1999, Masiello et al., 2015) associated to the non-linearity of the inverse problem in remote sensing (e.g.,Rodgers, 2000).

3.2. Calibration/Validation of the GSW Algorithm

The GSW parameters A_i, B_i, and C obtained by fitting equation (3) to the calibration dataset described in section 2.2. The GSW algorithm is verified against the independent subset of simulated TOA brightness temperatures comprised of all SeeBor profiles except for those selected for calibration (section 2.2). Figure 3 shows the error distribution of GSW LST models calibrated for Metop-A and Metop-B, respectively, within each class of W and SZA.

The overall bias of the GSW is -0.196ºC for Metop-A and -0.193ºC for Metop-B, while RMSE values are 0.553ºC and 0.541ºC for Metop-A and Metop-B, respectively. As shown in Figure 3, the retrieval errors tend to increase with both SZA and W. The RMSE is always below 2K for water vapour content and angles within the range of values admissible for Land-SAF ELST estimations, except for a few extreme cases with total column of water in the atmosphere close to 60 mm and view zenith angle at the edge of AVHRR swath.

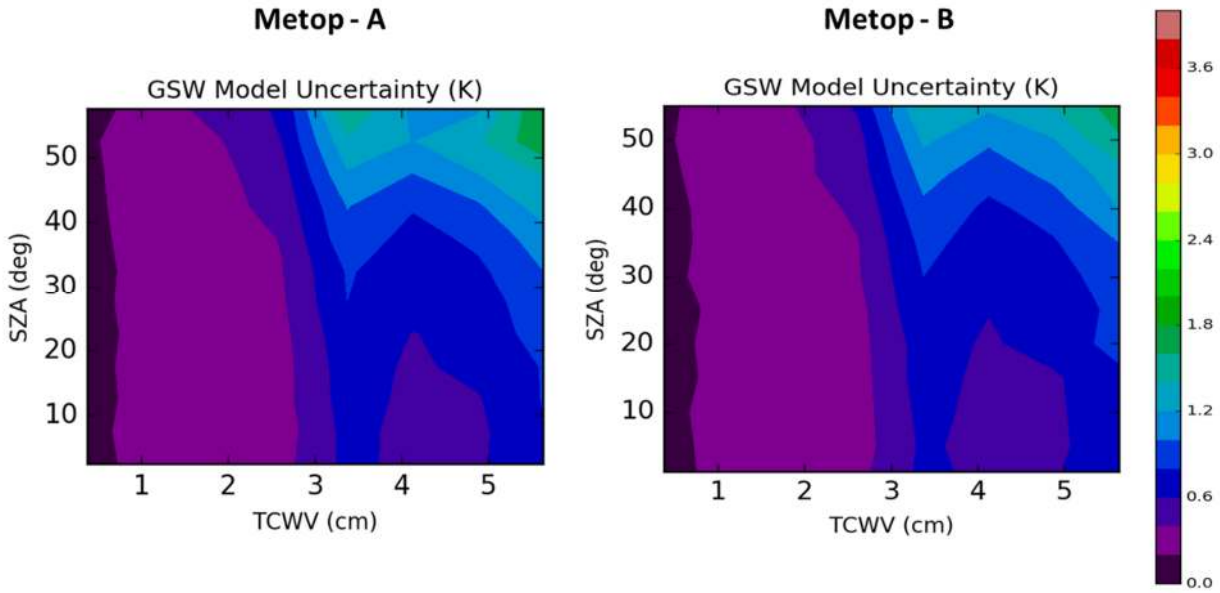


Figure 3 Assessment of the ELST Generalized Split-Windows algorithm against the validation databased: root mean square differences (ºC) per classes of Total Column Water vapour (x-axis) and view zenith angle (y-axis), considering the coefficients calibrated for Metop-A and Metop-B response functions, respectively.

4. Error Propagation

In a real scenario, we do not have access to the exact GSW inputs $X=(T_{10.8}, T_{12.0}, \varepsilon_{10.8}, \varepsilon_{12.0})$ and $Y=(W, \Psi)$, but only to inaccurate inputs, which we denote by $\hat{X}=(\hat{T}_{10.8}, \hat{T}_{12.0}, \hat{\varepsilon}_{10.8}, \hat{\varepsilon}_{12.0})$ and $\hat{Y}=(\hat{W}, \hat{\Psi})$. Therefore, if we still infer the LST according to model (3) replacing the exact GSW inputs with the inaccurate ones, we have a new source of error on the top of the fitting error ΔLST shown in Figure 3. In the current section, the main errors sources are identified and their impact on the total LST error estimated.

Potentially, all inputs may introduce errors in retrieved LST values. However, here we only consider the radiometric noise, the uncertainty in surface emissivity and errors in W forecasts. The misclassification of cloudy pixels as clear sky has very high impact on the retrieved LST. It is very difficult to propagate the uncertainty in cloud identification to LST uncertainty. Instead, users are recommended to be wary of LST retrievals in neighbouring cloudy pixels.

4.1. Framework

Let us define the vector of model coefficients $\theta=(A_1, A_2, A_3, B_1, B_2, B_3, C)$. Notice that, the vector θ generated by the fitting process is a function of water content and view angle, i.e., $\theta=\theta(Y)$. Consider the LST estimator $\hat{LST}=f(\hat{X},\hat{\theta})$ where $\hat{\theta}=\theta(\hat{Y})$ and $f(X,\theta)$ is the LST estimate given by model (3). A characterization of the model error is given by:

$$S_{LST}=E\left[\left(f(\hat{X},\hat{\theta})-LST\right)^2 \mid X,Y\right]^{1/2} \tag{4}$$

where $E[\cdot \mid X,Y]$ stands for mean value conditioned to X and Y; i.e., for a given GSW input X,Y, we want to compute the RMSE of the LST estimate. Using the fact that $LST=f(X,\theta)+\Delta LST$ and assuming that $E\left[f(\hat{X},\hat{\theta}) \mid X,Y\right]=f(X,\theta)$, we may write:

$$S_{LST}^2=E\left[\left(f(\hat{X},\hat{\theta})-f(X,\theta)\right)^2 \mid X,Y\right]+\Delta LST^2 \tag{5}$$

By taking a linear approximation of $f(\hat{X},\hat{\theta})$ in the neighbourhood of (X,θ), and denoting $\sigma_{X_i}^2=E\left[\left(\hat{X}_i-X_i\right)^2 \mid X\right]$ and $\sigma_{\theta_i}^2=E\left[\left(\hat{\theta}_i-\theta_i\right)^2 \mid Y\right]$, we are led to

$$S_{LST}^2=\sum_i\left(\frac{\partial f}{\partial X_i}\right)^2\sigma_{X_i}^2+\sum_j\left(\frac{\partial f}{\partial \theta_j}\right)^2\sigma_{\theta_j}^2+\Delta LST^2, \tag{6}$$

where we have assumed that the components of X , Y are mutually independent and that $E\left[\left(\hat{X}_i - X_i\right)| X\right] = 0$ and $E\left[\left(\hat{\theta}_i - \theta_i\right)| Y\right] = 0$. Next, we study in detail the error due to each individual GSW input.

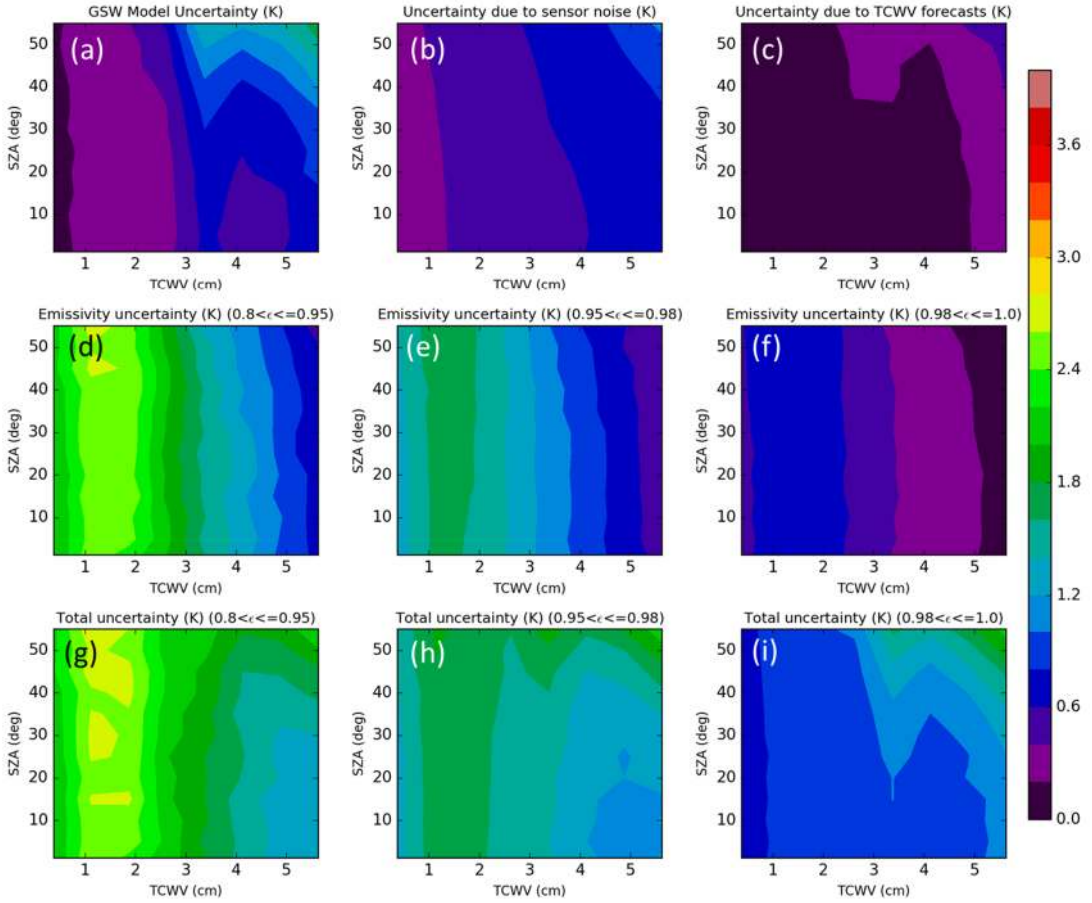


Figure 4 Uncertainty in LST estimates, measured as the RMSD (ºC) between retrieved LST and the validation database true value, considering: (a) the input data are error-free; (b) the sensor noise; (c) the uncertainty associated to total column water vapour forecasts; (d) uncertainty in surface emissivity, for cases where it lies between 0.8 and 0.95 (mostly barren surfaces); (e) uncertainty in surface emissivity, for cases where it lies between 0.95 and 0.98 (sparsely to moderately vegetated surfaces); (f) uncertainty in surface emissivity, for cases where it is higher than 0.95 (vegetated and/or moist surfaces or inland water bodies). The lower row represents total uncertainty, for the emissivity types described above. The results are presented for combinations of W (x-axis) and view zenith angle (y-axis), for Metop-B algoritm.

4.2. Impact of Sensor Noise

The expected radiometric noise of AVHRR channels 4 and 5 on-board Metop series is set 0.12ºC. The associated LST uncertainty is then

$$S_{Tb}^2 = S_{Tb4}^2 + S_{Tb5}^2 \tag{7}$$

where

$$S_{Tb4}^2 = \left(\frac{\partial f}{\partial T_4}\right)^2 \sigma_{T_4}^2 \quad \text{and} \quad S_{Tb5}^2 = \left(\frac{\partial f}{\partial T_5}\right)^2 \sigma_{T_5}^2 \tag{8}$$

Figure 4b shows the distributions of errors attributed to the impact of sensor noise, S_{Tb}, grouping all possible SZA within different ranges of W. S_{Tb}. is generally bellow 0.8ºC, and increases with the atmospheric water content.

4.3. Impact of uncertainties in Surface Emissivity

The impact of uncertainties in surface emissivity for channels 4 and 5, $\sigma_{\varepsilon 4}$ and $\sigma_{\varepsilon 5}$, respectively, on LST is given by:

$$S_{\varepsilon}^2 = S_{\varepsilon 4}^2 + S_{\varepsilon 5}^2 \tag{9}$$

where

$$S_{\varepsilon 4}^2 = \left(\frac{\partial f}{\partial \varepsilon_4}\right)^2 \sigma_{\varepsilon 4}^2 \quad \text{and} \quad S_{\varepsilon 5}^2 = \left(\frac{\partial f}{\partial \varepsilon_5}\right)^2 \sigma_{\varepsilon 5}^2. \tag{10}$$

Emissivity retrievals are based on the so-called Vegetation Cover Method (Caselles and Sobrino, 1989; Peres and DaCamara, 2005), where effective channel emissivity for any given pixel is estimated as a weighted average of channel emissivities of dominant bareground and vegetation types within the scene. Furthermore, it is considered that AVHRR pixels may include a land, F_{Land}, and and an in-land water fraction $(1 - F_{Land})$, and thus the effective pixel emissivity, ε_{eff_IRn}, is given by:

$$\varepsilon_{LAND_n} = \varepsilon_{veg_n} FVC + \varepsilon_{bg_n} (1 - FVC) \tag{11a}$$

$$\varepsilon_{eff_n} = \varepsilon_{LAND_n} F_{Land} + \varepsilon_{WATER_n} (1 - F_{Land}) \tag{11b}$$

where FVC is the pixel fraction of vegetation cover and ε_{veg_n}, ε_{bg_n}, ε_{WATER_n} are the vegetation, bareground, and water emissivities, respectively, for the split-window channel *n*. The values for ε_{veg_n} and ε_{bg_n} are available from look-up-tables, determined for the land cover classes within the IGBP (Belward, 1996) database (Peres and DaCamara, 2005); in the case of inland water, ε_{WATER_IRn} is set to the Water Bodies values, while pixels identified as snow/ice (either by the cloud mask algorithm or by the H-SAF snow products) are also set to the respective emissivity tabulated values. Channel emissivity is

to be estimated from FVC retrieved by the Land-SAF from AVHRR/Metop. It is however set to constant until this product is implemented in the production chain (see Table 3).

The uncertainties in retrieved emissivity are thoroughly discussed in (Trigo et al, 2008a). Emissivity uncertainties are higher for low emissivity surfaces (barre ground) and low for high emissivity surfaces (densely vegetated or water surfaces). The assessment of the impact assumed the following uncertainty values in surface emissivity (Table 2), estimated taking into account the variability of ε4 and ε5, as compiled from spectral databases (see Trigo et al., 2008a).

Table 2 Uncertainty values considered for surface emissivity of Metop channels 4 and 5.

Emissivity Ranges	Channel 4 $\sigma_{\varepsilon 4}$	Channel 5 $\sigma_{\varepsilon 5}$
$\varepsilon < 0.95$	0.030	0.025
$0.95 \le \varepsilon < 0.98$	0.020	0.010
$\varepsilon \ge 0.98$	0.006	0.006

Figure 4d, Figure 4e and Figure 4f show the results obtained for different ranges of surface emissivity. The results are shown taking into account the total column water vapour and satellite zenith angle. As expected, the sensitivity to land surface emissivity is significantly higher for drier atmospheres, since under moist conditions the impact of emissivity on the surface emitted radiance is partially compensated by an opposite effect on the (higher) atmospheric radiation reflected by the surface (Trigo et al., 2008a). Moreover, the higher values of $\sigma_{\varepsilon 4}$ and $\sigma_{\varepsilon 5}$ are found in (semi-)arid regions (Table 2), leading to LST inaccuracies of 1ºC or more under dry conditions (W below 2 cm). In contrast the impact on LST is always below 1.6ºC for the moister atmospheres (W > 4.5 cm).

4.4. Uncertainties in forecasts of atmospheric water vapour content

According to the equation (6), the error due to uncertainties in the water vapour content is given by:

$$S_W^2 = \sum_j \left(\frac{\partial f}{\partial \theta_j} \right)^2 \sigma_{\theta_j}^2 \tag{12}$$

where

$$\sigma_{\theta_j}^2 = E\left[\left(\hat{\theta}_j - \theta_j \right)^2 | W, \Psi \right] \tag{13}$$

Since we neglect the uncertainty in the SZA Ψ, let us focus out attention on *W*. Given that $\hat{\theta}$ is a piece-wise linear function, we have

$$\sigma_{\theta_j}^2 = E\left[\left(\hat{\theta}_j - \theta_j \right)^2 | W \right] = \sum_k \left(\hat{\theta}_j (R_k) - \theta_j \right)^2 P(\hat{W} \in R_k | W) \tag{14}$$

where R_k is the region of the water vapour domain where the k-th linear model is assumed. Therefore the sets R_k are a partition of the referred to domain.

The operational use of the GSW algorithm (3) to retrieve LST from AVHRR makes use of forecasts of total column water vapour (W) provided by the European Centre for Medium-range Weather Forecasts (ECMWF), for parameter selection. To characterize W error statistics, we compare ECMWF W forecasts (with forecast steps ranging between 12 and 36 h) with the respective analysis, for the 15th of each month for 1 full year, excluding cases with model cloud cover higher than 10%. This exercise is regularly (about once per year) to update the uncertainty in ECMWF forecasts.

The comparison between W forecasts and analysis (the reference value) allows us to estimate the probability $P(\hat{W}_i \mid W_j)$, i.e., the probability that $\hat{W}$ belongs to the water vapour content class W_i, given that the true class is W_j. This probability is then used to compute the expected LST error, according to the expressions (12) to (14). Figure 4c shows the impact on LST retrievals, which is exclusively attributed to forecast errors. These are generally very low, although they show an increase with the atmospheric moisture content.

4.5. Uncertainty of LST Retrievals

The estimation of LST error bars, S_{LST}, assumes that all sources of errors described in the previous sections are independent:

$$S_{LST} = \sqrt{S_{Tb}^2 + S_{\varepsilon}^2 + S_W^2 + \Delta LST^2} \tag{15}$$

Figure 4g, Figure 4h, and Figure 4i show the total uncertainty of LST for different scenarios of surface emissivity (and respective uncertainties). These were obtained for "LST retrievals" computed for the validation dataset described in section 2.2 and taking into account the uncertainties of the different input variables, as discussed above. Dry atmospheres present the widest range of S_{LST} in the case the surface emissivity is also low. Under such conditions, the total error depends essentially on emissivity uncertainties and to a lesser extent on the view zenith angle. For the case of high emissivity surfaces, S_{LST} increase with total water vapour content and view angle, i.e., LST error bars increase for higher optical depths.

The ELST product will be affected by large-scale systematic uncertainties. However, it should be stressed that the most likely source of systematic uncertainties in the LSA SAF LST products arises from systematic errors in surface emissivity. Given its low variability in time, errors in the bareground or vegetation emissivity attributed to any given pixel translates into a source of systematic errors, particularly relevant in arid and sparsely vegetated regions.

5. Daily Composites of AVHRR/Metop LST – LSA-002

The LSA SAF AVHRR/Metop LST product (ELST, product identifier LSA-002) consists of daily composites of LST values retrieved from individual AVHRR/Metop from individual Product Distribution Units, PDUs. The generalized split-window algorithm described above is applied to channel 4 and 5 top-of-atmosphere brightness temperatures, as described in the previous sections. Since the Fraction of Vegetation Cover (FVC) product based on AVHRR/Metop data has not yet been implemented, the current version of PDU-based LST is using a static emissivity map. This in turn is based on the land-cover classification of each pixel, according to the IGBP database, and on an average (fixed) value of the Fraction of Vegetation Cover attributed to each class following Peres and DaCamara (2005) (Table 3). The FVC values fixed in Table 3 are currently being used as input for the vegetation cover method used in the AVHRR/Metop LST processing, and will be replaced by the 10-daily LSA SAF FVC product which is planned to be derived from AVHRR (end of 2016).

Table 3 Fraction of Vegetation Cover attributed per land cover class.

IGBP Land Cover Class	Fraction of Vegetation Cover
1 – Evergreen Needle-leaf forest 2 – Evergreen Broad-leaf forest 3 – Deciduous Needle-leaf forest 4 – Deciduous Broad-leaf forest 5 – Mixed Forest 6 – Closed Shrubs	0.8
7 – Open Shrubs 8 – Woody Savannah 9 – Savannah 10 – Grasslands 12 – Croplands 14- Crops / Natural Vegetation	0.5
11 – Wetlands 15 – Snow/ ice 17 – water bodies	0
13 – Urban	0.1
16 – Barren	0.005

The estimation of LST uncertainty (error-bars) following the procedure described in section 4 will be implemented for the LST_AVHRR product only after the AVHRR/Metop FVC product is integrated into the LSA SAF system and the complete error propagation analysis described therein can be performed. At the moment, the LST_AVHRR (ELST, LSA-002) is distributed with a quality flag (Table 4), where providing qualitative information on the product quality. Taking into account the analysis of error propagation within the verification dataset, and the actual retrieval conditions (in terms of atmospheric moisture, viewing angle, and land-cover/emissivity), LST estimates are considered to be:

- Nominal when similar to conditions in validation database yield LST uncertainties between 1ºC and 2ºC.

- Below nominal when similar to conditions in validation database yield LST uncertainties above 2ºC.
- Above nominal when similar to conditions in validation database yield LST uncertainties below 1ºC.

Table 4- Description of LST/AVHRR Quality Flag information

Decimal Value	Description
-5	CMa - contaminated by snow/ice
-4	CMa - Cloud filled
-3	CMa - pixel contaminated by clouds
-2	Viewing Angle Out of Range
-1	Sea Pixel
0	Unprocessed pixel
1	Below Nominal
2	Nominal
3	Above Nominal

The PDU-based LST estimates are then organized by night-time and daytime values, according to the respective solar zenith angle (above or below 90º for night-time or daytime, respectively) and projected over a sinusoidal grid centred at (0ºN,0ºW), with a resolution of 0.01º by 0.01º. The projection to the sinusoidal grid is performed according to the following procedure:

1) we compute the location of the AVHRR/Metop pixel in the sinusoidal grid, ensuring that daytime and night-time AVHRR observations are treated separately.

2) we then consider all AVHRR LST pixels falling in the same grid-cell and the final LST value (as well as observation time and view zenith angle) will correspond to an average of all valid points; the QF will be set to the "worst" class; the number of original PDU pixels overlapping each sinusoidal grid-box is also provided

3) to avoid systematic gaps in the sinusoidal grid, we do a final check for non-filled grid cells; if these do not correspond to identified clouds/ sea pixels, they are filled in with an average of neighbouring points.

6. Concluding Remarks

The Generalised Split-Window (GSW) algorithm is a semi-empirical algorithm that allows the estimation of LST from top-of-atmosphere brightness temperatures of two adjacent channels within the atmospheric window part of the spectrum, assuming the channel surface emissivities are known. A version of the GSW was trained for AVHRR on-board the Metop series of satellites and is currently used for operational retrieval of AVHRR-based LST (ELST, LSA-002) by the Land-SAF. To maximize the algorithm performance over a wide range of conditions, the GSW parameters are tuned for classes of satellite view angle and total column water vapour (Martins et al, 2016). The algorithm

follows closely that first prepared for SEVIRI/MSG. Despite the higher spatial resolution and global coverage provided by AVHRR observations, this sensor presents poorer spectral information when compared with SEVIRI. In particular, the cloud screening, which is based on the software maintained by the NWC SAF, had to be necessarily adapted to the available channels. Information on atmospheric water content is obtained from ECMWF operational (hourly) forecasts and in the near future, the emissivity will be based on AVHRR estimates of FVC. Since this product has not been yet implemented in the LSA SAF system, a static FVC (and therefore emissivity) is being used at the moment, taking into account the pixel land cover classification.

The AVHRR LST product is made available as a daily composite (LSA-002), aggregating all daytime and night-time LST retrievals, respectively, over a full day – a 24-hour period between 00 UTC and 23:59 UTC. The product is currently distributed with a quality flag with qualitative information on the daily night-time/daytime estimates. An example of the ELST product and respective quality flag is presented in Figure 5 and Figure 6.

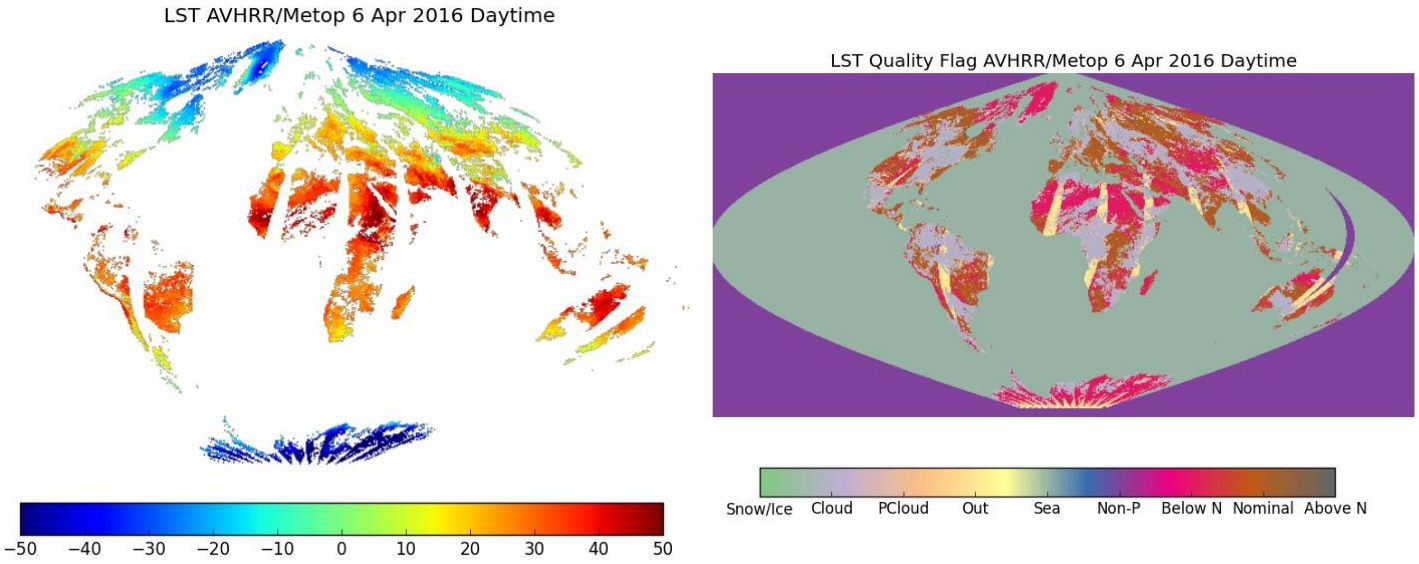


Figure 5 Example of one Daytime LST estimate (ºC) and respective quality flag.

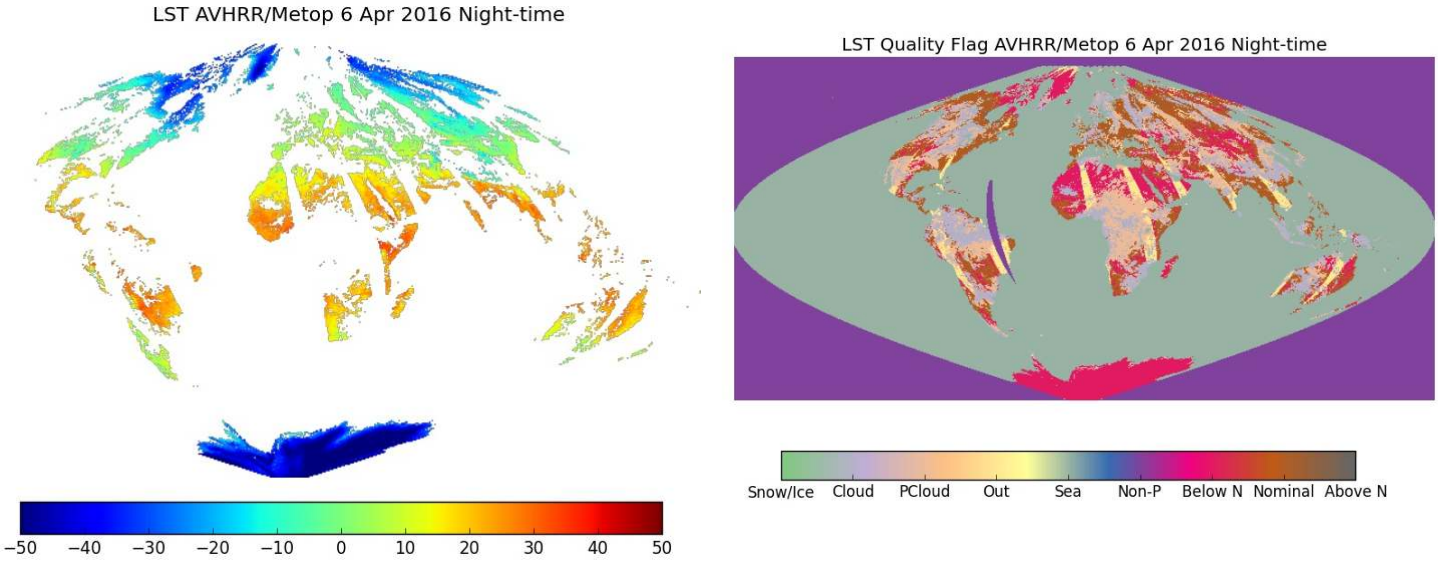


Figure 6 Example of one Night-time LST estimate (ºC) and respective quality flag.

7. References

Belward, A. S., "The IGBP-DIS global 1km land cover data set (DISCover) – proposal and implementation plans". IGBP-DIS working paper No. 13. IGBP-DIS Office, Météo-France, Toulouse, France, 61 pp, 1996.

Berk, A., G.P. Anderson, P.K. Acharya, J.H. Chetwynd, L.S. Bernstein, E.P. Shettle, M.W. Matthew, and S.M. Alder-Golden. "MODTRAN4 Version 2 User's Manual Air Force Res. Lab.", Space Vehicles Directorate, Air Force Material Command, Hanscom AFB, MA, 2000.

Borbas, E., S. W. Seemann, H.-L. Huang, J. Li, and W. P. Menzel, "Global profile training database for satellite regression retrievals with estimates of skin temperature and emissivity". *Proc. of the Int. ATOVS Study Conference-XIV*, Beijing, China, 25-31 May 2005, pp763-770, 2005.

Caselles, V. and J. A. Sobrino, "Determination of frosts in orange groves from NOAA-9 AVHRR data", *Remote Sens. Environ*., vol 29, 135–146, 1989.

Chevallier, F., "Sampled databases of 60-level atmospheric profiles from the ECMWF analyses", Numerical Weather Prediction Satellite Application Facility Research Report [NWP SAF Res. Rep.] no. 4, Jan 2002, 2001.

Chedin, A. N. A. Scott, C. Wahiche, and P. Moulinier, 1985, "The improved initialization inversion method: a high resolution physical method for temperature retrievals from satellites of the TIROS-N series", *J. Climate Appl. Meteor*., vol. 24, 128-143, 1985.

Coll, C., V. Caselles, J. M. Galve, E. Valor, R. Niclós, and J. M. Sánchez, "Evaluation of split-window and dual-angle correction methods for land surface temperature retrieval from Envisat/Advanced Along, Track Scanning Radiometer (AATSR) data", *J. Geophys. Res.,* vol. 111, D12105, doi:10.1029/2005JD006830, 2006.

Dash, P., F. M. Göttsche, F. S. Olesen and H. Fischer, "Land surface temperature and emissivity estimation from passive sensor data: theory and practice–current trends", *Int. J. Remote Sens*., vol. 23, 2563–2594, 2002.

Dybbroe, A., K.-G. Karlsson, and A. Thoss, "NWSAF AVHRR cloud detection and analysis using dynamic thresholds and radiative transfer modeling. Part I: Algorithm description". *J. Appl. Meteor*., **44**, 39–54, 2005.

EUMETSAT, AVHRR Level 1b Product Guide, EUM/OPS-EPS/MAN/04/0029, v3A, 2011.

Faysash A. and E. A. Smith, "Simultaneous land surface temperature-emissivity retrieval in the infrared split window". *J. Atmos. Oceanic Technol*., vol. 16, 1673-1689, 1999.

Jiang, G.-M. and Z.-L. Li, "Split-window algorithm for land surface temperature estimation from MSG1-SEVIRI data", *Int. J. Remote Sens*., vol 29, 6067–6074, 2008.

Jiménez-Muñoz, J. C. and J. A. Sobrino, "Error sources on the land surface temperature retrieved from thermal infrared single channel remote sensing data", *Int. J. Remote Sens*., vol 25, 999–1014, 2006.

Masiello, G., C. Serio, S. Venafra, G. Liuzzi, F. Göttsche, I. F. Trigo, and P. Watts, "Kalman filter physical retrieval of surface emissivity and temperature from SEVIRI infrared channels: a validation and intercomparison study", *Atmos. Meas. Tech*., **8**, 2981–2997, doi: 10.5194/amt-8-2981-2015, 2015.

Martins, J. P. A., I. F. Trigo, V. A. Bento, and C. da Camara , "A Physically Constrained Calibration Database for Land Surface Temperature Using Infrared Retrieval Algorithms", *Remote Sensing*, **8**, 808; doi:10.3390/rs8100808, 2016.

Peres, L. F. and C. C. DaCamara, "Emissivity Maps to Retrieve Land-Surface Temperature From MSG/SEVIRI", *IEEE Trans. Geosci. Remote Sens*., vol. 43, pp. 1834-1844, 2005.

Prata, A. J. "Land surface temperature derived from the advanced very high resolution radiometer and the along-track scanning radiometer: 1. Theory", *J. Geophys. Res*., vol. 98, 16,689– 16,702, 1993.

Rodgers, C. D., "Inverse methods for atmospheric sounding: theory and practice", Series on Atmospheric, Ocean and Planetary Physics, vol. 2. World Scientific, Hackensack, 238 pp., 2000.

Seemann, S. W., J. Li, W. P. Menzel, and L. E. Gumley, "Operational retrieval of atmospheric temperature, moisture, and ozone from MODIS infrared radiances". *J. Appl. Meteor*., vol 42, 1072-1091, 2003

Sobrino, J.A., M. Romaguera, "Land surface temperature retrieval from MSG1-SEVIRI data", *Remote Sens. Environ*., vol 92, 247–254, 2004.

Sun, D. and R. T. Pinker, "Estimation of land surface temperature from a Geostationary Operational Environmental Satellite (GOES-8)", *J. Geophys. Res*., vol. 108, 4326, doi: 10.1029/2002JD002422, 2003.

Trigo, I. F. and P. Viterbo, "Clear-Sky Window Channel Radiances: A Comparison between Observations and the ECMWF Model", *J. Appl. Meteor.*, vol. 42, 1463–1479, 2003

Trigo, I. F., L. F. Peres, C. C. DaCamara, and S. C. Freitas, "Thermal Land Surface Emissivity Retrieved From SEVIRI/Meteosat.", *IEEE Trans. Geosci. Remote Sens*., vol 46, doi: 10.1109/TGRS.2007.905197, 2008a.

Trigo, I. F., I. T. Monteiro, F. Olesen, and E. Kabsch, "An assessment of remotely sensed Land Surface Temperature", *J. Geophys. Res*., vol 113, D17108, doi:10.1029/2008JD010035, 2008b.

Wan, Z. and J. Dozier, 1996, "A generalized split-window algorithm for retrieving land surface temperature from space", *IEEE Trans. Geosci. Remote Sens*., vol. 34, 892–905, 1996.

Yu, Y., J. L. Privette, and A. C. Pinheiro, "Evaluation of Split-Window Land Surface Temperature Algorithms for Generating Climate Data Records", *IEEE Trans. Geosci. Remote Sens*., vol. 46, doi: 10.1109/TGRS.2007.909097, 2008.